Acta Cryst. (1981). A**37**, 229–238

Ca and Na Positions in Labradorite Feldspar as Derived from High-Resolution Electron Microscopy and Optical Diffraction

BY A. KUMAO

Department of Physics, Kyoto Technical University, Kyoto 606, *Japan*

H. HASHIMOTO

Department of Applied Physics, Osaka University, Suita, Osaka 565, *Japan*

H.-U. NISSEN

Laboratorium für Festkörperphysik, Eidgenössische Technische Hochschule, CH-8093 *Zürich, Switzerland*

AND H. ENDOH

Department of Applied Physics, Osaka University, Suita, Osaka 565, *Japan*

(*Received* 19 *June* 1979; *accepted* 27 *August* 1980)

Abstract

A model for the Ca/Na positions in the superstructure of labradorite in low structural state (*i.e.* having *e*-type satellite reflections) with approximately 50 mol% anorthite is proposed on the basis of high-resolution electron microscopic structure images and a comparison of the corresponding electron diffraction patterns with optical diffraction patterns obtained from masks made to represent projections of the structure models with the diameter of the holes representing the scattering factors of the atoms. Good agreement in corresponding positions is found between these optical diffraction patterns and the electron diffraction patterns for projections along the four different axes [010], [311], [131] and [5$\bar{1}$1]. The Al/Si atoms influence the diffraction pattern only with regard to a few indices, thus the correspondence of optical and electron diffraction patterns is increased by including Al and Si. The model agrees with the known average structure of labradorite (An53) but differs from models proposed previously for the diffraction satellites and the antiphase boundaries causing them.

1. Introduction

The chemically intermediate plagioclase feldspars including labradorite have a complicated superstructure associated with satellites in X-ray and electron diffractograms. Both the positions and the intensities of these incommensurate satellites change with the Ca/Na and Al/Si proportions, respectively. The problem of determining the positions of the atoms, especially Ca and Na, from the properties of the *e*-type and *f*-type satellites (nomenclature of Bown & Gay, 1958) has been attacked by X-ray crystallographers since the early attempt of Megaw (1960). Later, a number of different models for the Ca/Na positions were proposed by Korekawa and his collaborators (Korekawa & Jagodzinski, 1967; Korekawa & Horst, 1974; Jagodzinski & Korekawa, 1976, 1978; Korekawa, Horst & Tagai, 1978). Different proposals for the Ca/Na and, in part, the Al/Si positions were made by Toman & Frueh (1973*a*,*b*, 1976*a*,*b*), Hashimoto, Kumao, Endoh, Nissen, Ono & Watanabe (1975), Kitamura & Morimoto (1977) and Grove (1977). Klein & Korekawa (1976) have found the Ca/Na position to be split.

In view of the significant differences between the various models based on X-ray diffraction, it was hoped that new techniques of high-resolution electron microscopy, *i.e.* multibeam structure imaging, might provide independent information on the atomic positions in labradorite. Such images with a point-to-point resolution of between 3 and 4 Å were first made by Hashimoto *et al.* (1975) and Hashimoto, Nissen, Ono, Kumao, Endoh & Woensdregt (1976), and a similar image was published by Morimoto, Nakajima & Kitamura (1975) and Morimoto, Kitamura & Nakajima (1975). The works of McLaren & Marshall (1974), McConnell (1974), Wenk, Wenk, Glauser & Schwander (1975) and Wenk (1978), giving information on the fringes in electron micrographs associated with the *e*-type satellite reflections of labradorite, are also pertinent.

In this paper, electron diffraction patterns of the specimen area corresponding to the multibeam struc-

0567-7394/81/020229-10$01.00

ture images are compared with optical diffraction patterns made with a He–Ne laser of two-dimensional structure projection models consisting of circular holes representing the atoms (Lipson, 1972). It is shown firstly by the contrast calculation that the contrast difference between Ca and Na atoms in structure images is sufficiently strong to allow a study of the occupancy of the Ca/Na atoms, and secondly that good correspondence exists between optical diffraction patterns from a two-dimensional structure projection model or an electron micrograph taken in optimum focus conditions and electron diffraction patterns from a thin crystal. On this basis, a model for the positions of Ca and Na atoms in labradorite of approximately An50 composition is proposed. The influence of the tetrahedral atoms (Al and Si) on the diffraction pattern is also investigated, and the model is briefly compared to proposals for the labradorite structure made in previous publications.

2. Contrast difference between Ca and Na atoms in structure images of labradorite

Electron waves which are incident on thin crystals are scattered by the electric potential field formed by atoms and are projected as the interference fringes at the bottom surface of the crystal. For very thin crystals which consist of light atoms and can be considered as weak phase objects, the contrast of the interference fringes is proportional to the potential distribution in the crystal, *i.e.* the projected potential (Cowley, 1959). In the electron microscopic images of crystals, the intensity distribution of electron waves at the bottom surface of the crystal is projected on the image plane by the electron lenses with aberrations. In the optimum focus condition (Scherzer, 1949), the effect of spherical aberration can be eliminated and the intensity distribution of the images becomes proportional to the potential distribution.

For crystals with realistic thickness, the intensity distribution of electron waves at the bottom surface of the crystal is not precisely proportional to the potential distribution in the crystal. The deviation is chiefly due to the interference of electron waves scattered from the adjacent atoms. The contrast of the images of Ca and Na atoms in the labradorite feldspar has been studied by the present authors using the many-beam dynamical theory (eigenvalue equation method) and a model in which, by a simplified assumption, 50% of the Ca atoms in the anorthite structure were replaced by Na atoms (Hashimoto *et al.*, 1975). Fig. 1(*a*) shows the model mentioned above and Fig. 1(*b*) is the computed image of the model for a crystal 60 Å thick formed by a real lens ($C_s = 0{\cdot}7$ mm) at the defocus $\Delta f = 600$ Å. 107 waves were excited and 22 waves contributed to the image by passing through the objective aperture. This imaging condition is identical to that for the present electron microscopic observations. The arrows in Fig. 1 show the positions of Ca and Na atoms. As can be seen in Fig. 1(*b*), the image contrast in the positions of the Ca atoms is darker than that in Na atom positions. Therefore, it may be reasonable to assume that Ca atoms cause darker contrast than Na atoms in the images of labradorite if the thickness of the crystal is around 60 Å.

3. Relations between electron diffraction patterns of thin crystals and optical diffraction patterns obtained from many-beam structure images or two-dimensional models of structure projections

The optical diffraction patterns made from high-resolution electron micrographs of crystals (in the form of the original negative of the electron micrograph) can be used to obtain crystallographic information provided that the electron micrograph is made under optimum focus conditions (Tanji & Hashimoto, 1978). If the object is a thin crystal which may be assumed to be a weak phase object ('weak phase grating approximation'), its transmission function $q(x,y)$ can be written as

$$q(x,y) = 1 - i\sigma\varphi(x,y), \qquad (1)$$

where σ is the interaction constant and $\varphi(x,y)$ is the projected potential along the direction of the incident beam. The amplitude of the corresponding electron diffraction pattern is expressed by the Fourier trans-

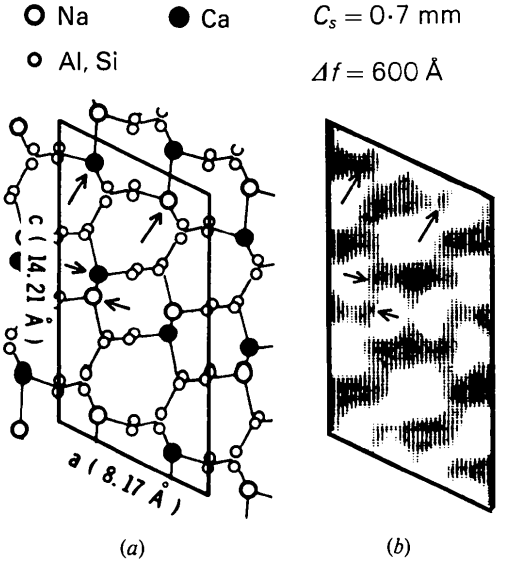

Fig. 1. (*a*) Projection onto the *ac* plane of an anorthite-like structure having 50% Na atoms instead of Ca atoms. Thin lines demonstrate the ring-like arrangement of atoms in the projection and do not represent individual bonds. (*b*) Calculated image contrast.

form of (1), and the intensity $E(u,v)$ is given by the square of the amplitude:

$$E(u,v) = \delta(u,v) + \sigma^2 \Phi^2(u,v), \quad (2)$$

where $\Phi(u,v)$ is the Fourier transform of $\varphi(x,y)$ and $\delta(u,v)$ is a delta function in two dimensions. The intensity $I_i(x_i,y_i)$ of the electron microscopic image is given by the square of the Fourier transform of the wave function for the electron diffraction pattern as

$$I_i(x_i,y_i) = 1 - 2\sigma\varphi(x_i,y_i) * \mathcal{F}(\sin\gamma), \quad (3)$$

γ is the phase shift at the back focal plane of the objective lens and is given by

$$\gamma = \frac{\pi}{2\lambda}(C_s\alpha^4 - 2\Delta f\alpha^2), \quad (4)$$

where λ, C_s, α and Δf are the wavelength, the spherical aberration coefficient, the scatter angle of the incident beam and the amount of defocus, respectively. The intensity $L(U,V)$ of the optical diffraction pattern made from the electron micrograph, of which the intensity is expressed by (3), is given by

$$L(U,V) = \delta(U,V) + 4\sigma^2 \Phi^2(U,V)\sin^2\gamma. \quad (5)$$

By comparing (5) with (2) it is evident that $L(U,V)$ is proportional to $E(u,v)$ if $\sin^2\gamma = 1$. This is the case for the 'optimum focus condition' (Scherzer, 1949), and for this focus condition the optical diffraction pattern is identical to the electron diffraction pattern of the same area of the crystal. However, it should be noted that this relation is only valid for very thin crystals, *i.e.* for the case where the weak phase object (WPO) approximation holds. For the interpretation of the images of labradorite crystals around 60 Å thick, the phase object approximation may be adequate rather than the WPO approximation. The failure of the WPO approximation will have some effect on the diffraction intensities, but it can be emphasized that it will not change the symmetry indication, such as forbidden reflections, and will give roughly the right relative intensities.

This identity of electron diffraction patterns and optical diffraction patterns is also limited by the mechanism of the scattering process. The electron diffraction phenomenon in a thin crystal is due to scattering of electrons by atoms arranged in three dimensions, whereas the optical diffraction phenomenon is due to scattering of a light beam by a two-dimensional array of small holes. The scattering amplitudes of Ca and Na atoms for electrons are shown in Fig. 2(*a*). The scattering amplitude of the Ca atom is about twice that of the Na atom for all scattering angles. On the other hand, when a light beam is incident on a circular aperture of radius a, the amplitude diffracted in the direction of the angle θ is, as generally known, given by

$$A(\theta) = C(\pi a^2)\left\{\frac{2J_1[(2\pi a\sin\theta)/\lambda]}{(2\pi a\sin\theta)/\lambda}\right\}, \quad (6)$$

where λ is the wavelength of light and $J_1(x)$ is the first-order Bessel function. Since the function $J_1(x)/x$ has the value zero at $x = 1{\cdot}220\pi$, $2{\cdot}233\pi$, $3{\cdot}234\pi$, ..., the diffraction spots due to a two-dimensional array of holes with radius a are extinguished at specific θ angles, *i.e.* the radius of the first dark ring is given by $1{\cdot}22/(2a)$. In order to observe the diffraction spots clearly, for example up to the third-order reflections of lattice planes with spacing d, $3/d$ must be smaller than $1{\cdot}22/(2a)$, *i.e.* $a < 0{\cdot}2d$. As can be seen in (6), the amplitude is proportional to the area of the aperture. Therefore, in optical models representing the crystal structure the ratio of the radii of holes representing Na and Ca atoms must be $1:\sqrt{2}$ because the ratio of the atomic scattering amplitudes of Na and Ca atoms is about 1:2. The light scattering amplitudes from the two apertures with the radius ratio $1:\sqrt{2}$ are shown in Fig. 2(*b*), which suggests that the amplitude ratio is 1:2 for small scattering angles and becomes 1:1 at the specific angle α. Therefore, the optical diffraction pattern can be used only within a range up to a maximum angle α for investigating electron diffraction patterns. This is valid not only with regard to spacing but also to intensity.

In the present study, the columns of atoms are represented by holes, the diameters of which are proportional to the square root of the scattering amplitude of that atom. The positions of atoms in the crystal which contribute to the phases of the diffracted waves are represented by the positions of the holes. For the superposition of Ca and Na atoms, the scattering amplitudes are taken as the average of the individual atoms. This representation of atoms in the crystal is

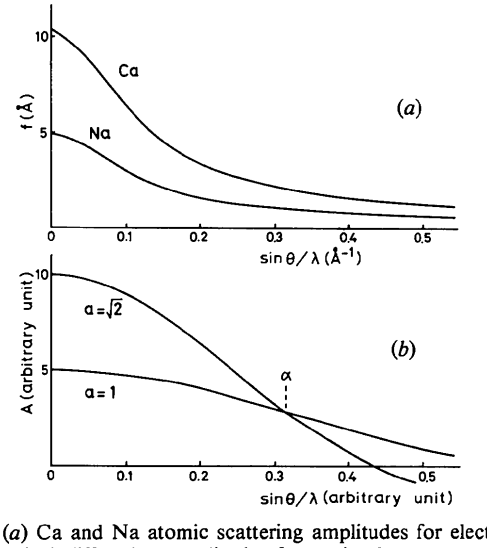

Fig. 2. (*a*) Ca and Na atomic scattering amplitudes for electrons. (*b*) Optical diffraction amplitudes for a circular aperture. The ratio of the radii of the apertures is $\sqrt{2}:1$.

called a 'mat' and is used to obtain an optical diffraction pattern. The optical model and hence the mat was corrected after comparing the optical diffraction pattern with the electron diffraction pattern or the optical diffraction pattern made from electron micrographs taken at the optimum focus condition.

4. Crystallographic data used for the present experiment

The specimen, No. 1513c, of labradorite An54 from Labrador was used for electron microscopic observations. Although the exact coordinates of all atoms in intermediate plagioclase are unknown, the atomic coordinates of the averaged structure of An55 proposed by Toman & Frueh (1973*a*) for space group $C1$ with a subcell $c = 7$ Å were used to construct optical models of the atomic occupancy. For constructing the present model, the anorthite cell was used, with $a = 8{\cdot}17$, $b = 12{\cdot}86$, $c = 14{\cdot}22$ Å; $\alpha = 93{\cdot}6$, $\beta = 116{\cdot}2$, $\gamma = 89{\cdot}8°$. Eight Ca/Na atom positions are derived in a 14 Å unit cell by translations of $\mathbf{c}/2$, $(\mathbf{a} + \mathbf{b})/2$ and $(\mathbf{a} + \mathbf{b} + \mathbf{c})/2$ after Korekawa & Jagodzinski (1967) and shown in Table 1. The positions of Ca and Na atoms were derived from the electron micrographs (Hashimoto *et al.*, 1975) as will be discussed in detail. The final model refined by the present experiment will be described in § 6.

In Fig. 3 1, 1′, 2 and 2′ each refer to a Ca/Na single atom, *i.e.* the black and the shaded discs refer to Ca and Na atoms, respectively, and the reverse is also true. Fig. 4 shows the Ca/Na positions in a unit cell projected onto the planes normal to the axes [010], [131], [5$\bar{1}$1] and [311]. These axes are parallel to the electron beam for the structure imaging of labradorite used in the present study. The circular areas surrounded by dotted lines represent the projected positions of all Ca/Na atoms contained within the adjacent unit cells in the crystals. It can be noted from Fig. 4 that atoms 1 and 1′ in any unit cell are lying on a straight line on the projection planes mentioned above. Atoms 2 and 2′ are projected on another line which is parallel to that of atoms 1 and 1′. Similar lines exist for the other pairs of positions, *i.e.* 3–3′ and 4–4′ are parallel to 1–1′. All these lines were always constructed for each of the structure projections and are parallel to a specific plane. For the projections along the axes [010] and [131], the specific plane is the (10$\bar{1}$) plane, which is parallel to the *b* axis and perpendicular to the projection planes. The atom line 1–1′ appears close to the atom line 2–2′ and the atom line 3–3′ appears close to the atom line 4–4′. For the projections along the axes [5$\bar{1}$1] and [311], the specific planes are the (011) plane and the (00$\bar{1}$) plane respectively, both of which are parallel to the *a* axis and perpendicular to the projection planes. In these projections, the atom line 1–1′ appears close to the atom line 3–3′, and 2–2′ close to 4–4′.

Table 1. *Atomic coordinates of* Ca/Na *in anorthite cell*

Indices in the left column refer to each atom.

Ca/Na	*x*	*y*	*z*
1	0·2689	0·9767	0·0832
1′	0·7689	0·4767	0·5832
2	0·7305	0·9729	0·4463
2′	0·2305	0·4729	0·9463
3	0·7305	0·9729	0·9463
3′	0·2305	0·4729	0·4463
4	0·2689	0·9767	0·5832
4′	0·7689	0·4767	0·0832

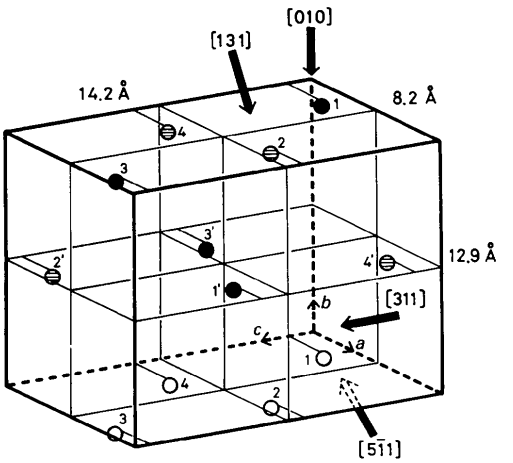

Fig. 3. Atom positions of Ca/Na in the anorthite cell. Black discs represent Ca, shaded discs Na. The case in which all Ca atoms are replaced by Na and *vice versa* also represents the structure.

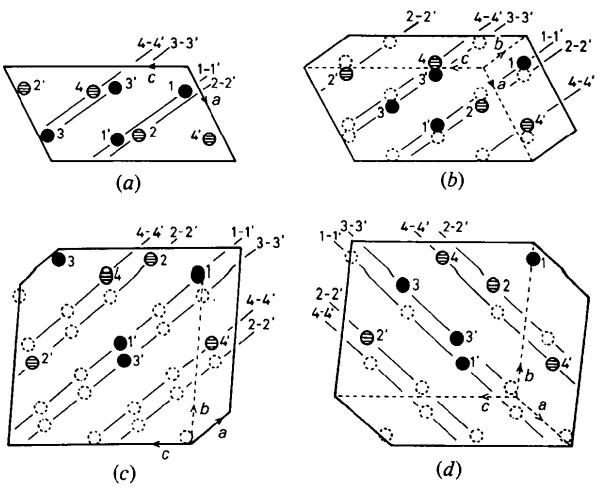

Fig. 4. Ca/Na atom positions in one anorthite unit cell projected onto the planes normal to (*a*) [010], (*b*) [131], (*c*) [5$\bar{1}$1] and (*d*) [311]. The dotted line circles represent the positions of Ca/Na atoms contained within all adjacent unit cells.

5. Structure images and diffraction patterns

The labradorite sample in the form of small powder fragments supported by holey carbon foils was investigated in a JEM 100C electron microscope with a spherical aberration coefficient $C_s = 0{\cdot}7$ mm and 100 kV voltage. The specimen has An54 mol% composition and has been described in detail in a previous publication (Hashimoto *et al.*, 1976). Through-focus series of electron microscope images were taken in four orientations, *i.e.* [010], [131], [5$\bar{1}$1] and [311] for specimen thicknesses between 50 and 100 Å, and structure images (optimum focus condition) resulted in an underfocus of around −900 Å.

In each of Figs. 5–7, the multibeam electron microscopic structure image and the corresponding electron diffraction pattern are shown together with a model of the structure projection made as outlined in § 4 as well as the optical diffraction patterns made from the electron micrograph and the model. In the electron micrographs steps in the bands of dark contrast divide the area into domains with boundaries approximately parallel to (11$\bar{4}$). This boundary is perpendicular to the plane of the micrograph for the projections along [131], [5$\bar{1}$1] and [311]. Fig. 5 shows the case of the projection along [311]. An electron micrograph is shown in Fig. 5(*a*) (this and the following micrographs should be looked at edge-on in the vertical direction in order to recognize the step structure). It shows dark spots arranged in lines parallel to the projection of the (01$\bar{1}$) plane. A comparison of the contrast of the micrograph shown in Fig. 5(*a*) with the atom projection shown in Fig. 4(*d*) allows the assumption that atoms 1, 1′, 3 and 3′ are Ca and atoms 2, 2′, 4 and 4′ are Na. (These atoms are marked as black and shaded discs in Figs. 3 and 4.) This assumption is based on the fact that atom rows 1–1′ and 3–3′ are adjacent to each other and appear as dark bands, while atom rows 2–2′ and 4–4′ form bands of lighter(grey) contrast. The contrast of these bands also indicates that all Ca positions are replaced by Na every nine anorthite subcells in a direction parallel to the *a* axis and all Na positions by Ca. Fig. 5(*b*) gives the model of the projected Ca/Na positions on the same scale as Fig. 5(*a*). The projection of the (11$\bar{4}$) plane and the nomenclature of atoms are indicated at the lower margin of Fig. 5(*b*). In Fig. 5(*c*) an optical diffraction pattern is given, which was obtained from the original negative film used to make Fig. 5(*a*). Fig. 5(*d*) shows the electron diffraction pattern corresponding to Fig. 5(*a*) but from a larger area, and Fig. 5(*e*) is an optical diffraction pattern made from the model shown in Fig. 5(*b*). By comparing Fig. 5(*e*) with Figs. 5(*c*) and (*d*), it is clearly seen than *a* and *e* spots appear in similar positions except for two missing 130 and 130 spots. The absence of these spots is due to the distance of a pair of holes used in the model (*b*), which will be discussed in § 6. Many other optical models besides that shown in Fig. 5(*b*) can produce a pattern similar to that shown in Fig. 5(*e*), but the model shown in Fig. 5(*b*) is the only one which does not contradict the image shown in Fig. 5(*a*) and the crystal structure model given by Toman & Frueh (1973*a*). The deviation in the direction connecting pairs of *e*-type satellites in Figs. 5(*c*) and (*d*) compared to Fig. 5(*e*) is due to a small difference in the orientation of the domain boundaries. This is frequently found in labradorites as a result of small-scale structural or chemical inhomogeneities.

Fig. 6 shows the case of the projection along [131]. The dark spots in the electron micrograph, Fig. 6(*a*), are arranged parallel to the projection of the (10$\bar{1}$) plane. From observation of the image, it appears that the positions of Na and Ca atoms are exchanged every nine unit cells along the *b* axis. Since for this projection the positions of the Ca and the Na atoms are very close, the difference in contrast between bands of Ca and those of Na is less pronounced, and the dark regions in Fig. 6(*a*) show some fluctuation along (10$\bar{1}$). Fig. 6(*b*) shows the model of the projected Ca/Na positions. Fig. 6(*c*) shows the optical diffraction pattern of the image represented in Fig. 6(*a*). The electron

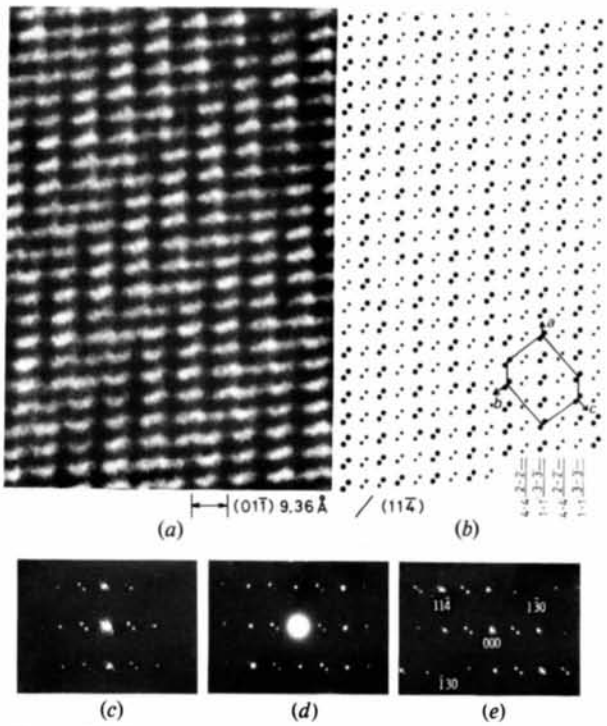

Fig. 5. (*a*) Electron micrograph of labradorite An54 oriented with its axis [311] parallel to the electron beam. (*b*) A model tested by optical diffraction. Large discs represent the superposition of two Ca atoms, intermediate discs one Ca and one Na, small discs two Na atoms. These representations are the same as in Figs. 6(*b*) and 7(*b*). (*c*) Optical diffraction pattern made from the micrograph in (*a*). (*d*) Electron diffraction pattern corresponding to the image in (*a*). (*e*) Optical diffraction pattern of the model in (*b*).

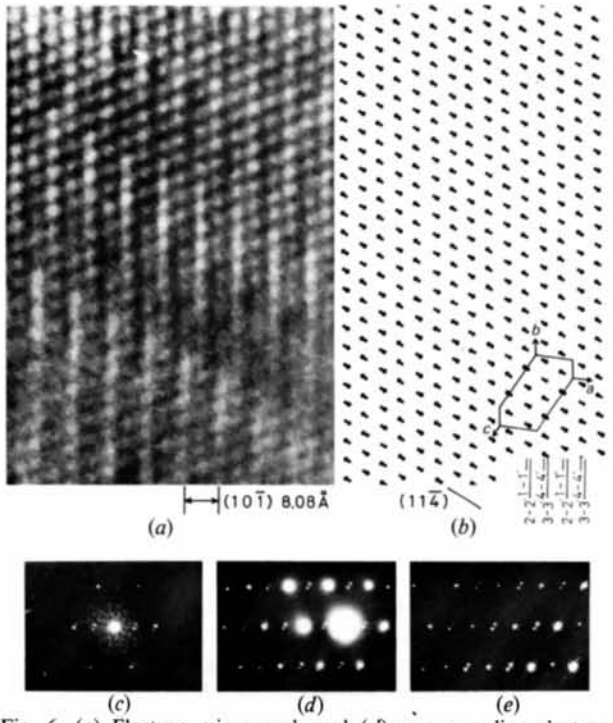

Fig. 6. (*a*) Electron micrograph and (*d*) corresponding electron diffraction pattern of labradorite oriented with its axis [131] parallel to the electron beam. (*b*) A model projected onto the plane normal to the axis [131]. (*c*), (*e*) Optical diffraction patterns of the image in (*a*) and the model in (*b*), respectively.

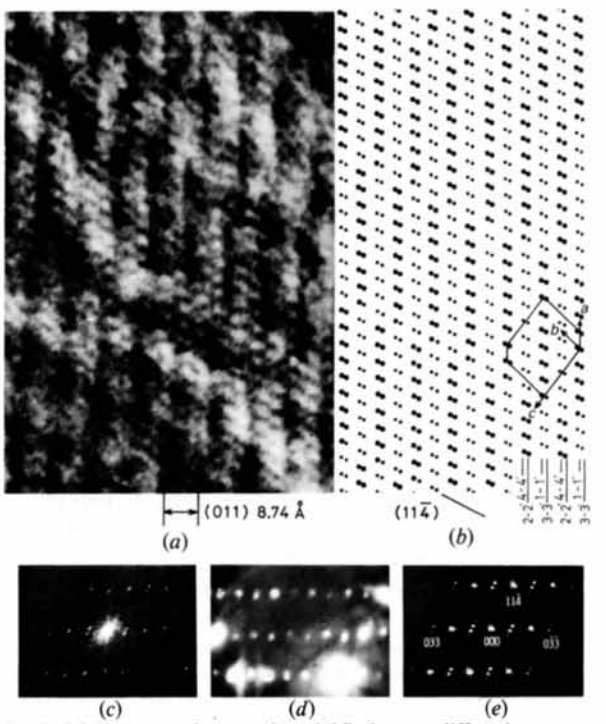

Fig. 7. (*a*) Electron micrograph and (*d*) electron diffraction pattern of labradorite oriented with its axis [5$\bar{1}$1] parallel to the electron beam. (*b*) An arrangement of Ca and Na atoms projected onto the plane normal to the axis [5$\bar{1}$1]. (*c*), (*e*) Optical diffraction patterns of the image in (*a*) and the model in (*b*), respectively.

diffraction pattern is shown in Fig. 6(*d*), and Fig. 6(*e*) shows the optical diffraction pattern made from the model, Fig. 6(*b*). Intensity differences of spots which were discussed in Fig. 5 are also seen in Figs. 6(*d*) and (*e*).

Fig. 7 shows the third case, *i.e.* the projection along [5$\bar{1}$1]. As seen from the electron micrograph, Fig. 7(*a*), as well as the model of the projected Ca/Na positions, Fig. 7(*b*), there is a relatively large distance of the double rows of projected atoms associated with Ca and Na, respectively. The dark spots in Fig. 7(*a*) are arranged in lines parallel to the projection of the (011) plane. Fig. 7(*c*) shows an optical diffraction pattern made from the negative of the electron micrograph. Fig. 7(*d*) gives the electron diffraction pattern corresponding to Fig. 7(*a*). The spots are rather large in this diffraction pattern because a large beam divergence was chosen. One of the *e* satellites in the satellite pairs is frequently missing due to a tilt deviation of the crystal away from the exact orientation. These two deficiencies of Fig. 7(*d*) have to be taken into account when Fig. 7(*d*) is compared with both Figs. 7(*c*) and (*e*). The latter figure shows the optical diffraction pattern made from the model, Fig. 7(*b*).

6. Construction of a model for the Ca/Na positions in labradorite

The superpositions of Ca and Na atoms in the projections along [311], [131] and [5$\bar{1}$1] can be found as shown in Fig. 8 by considering the positions of individual atoms in a number of adjacent anorthite unit cells. For the projection along [311] shown in Fig. 8(*a*), the superposition is found by shifting an anorthite cell along the *a* axis in steps of one unit length, so that identical atoms are repeated every three layers. The ratio of the atom groups 1–1′, 2–2′, 3–3′ and 4–4′ and hence the bulk projected potential along the [311] direction will not change when the thickness of the specimen is increased. Similarly, identical atoms are repeated every three and five layers for the projections along [131] and [5$\bar{1}$1] respectively, as shown in Figs.

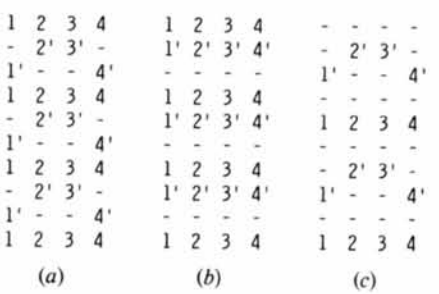

Fig. 8. The superpositions of Ca/Na atoms in the projections along (*a*) [311], (*b*) [131] and (*c*) [5$\bar{1}$1]. Indices refer to each atom. Identical atoms are repeated every three layers for the projections along [311] and [131], and every five layers for [5$\bar{1}$1].

8(*b*) and (*c*). The optical models used for Figs. 5, 6 and 7 were made by the superposition of repeat unit layers (three or five layers).

If the antiphase domain boundary is exactly lying in $(11\bar{4})$ which is parallel to the axes [311], [131] and $[5\bar{1}1]$, the atoms within the anorthite subcells whose origins are located at $n(\mathbf{a} - \mathbf{b})$, where n is an integer, must have the same occupancy as in the anorthite subcell at the origin. Similarly, the subcells located at $n(\mathbf{c} + 4\mathbf{a})$ and $n(\mathbf{c} + 4\mathbf{b})$ must have the same occupancy as the subcell at the origin, because the origins of all subcells located at $n(\mathbf{a} - \mathbf{b})$, $n(\mathbf{c} + 4\mathbf{a})$ and $n(\mathbf{c} + 4\mathbf{b})$ are in the same plane parallel to $(11\bar{4})$. Fig. 9 shows the model constructed after the rules outlined above and the replacement of the positions of Ca or Na atoms every nine subcells along the *a* and *b* axes. In the white regions of the drawing, positions 1, 1′, 3 and 3′ are occupied by Ca and positions 2, 2′, 4 and 4′ by Na. In the dark regions the occupancy is in antiphase relation, *i.e.* positions 1, 1′, 3 and 3′ are occupied by Na, and positions 2, 2′, 4 and 4′ by Ca. A drawing of this simple model, which is shown in Fig. 10(*a*), was obtained by projecting only those Ca and Na atoms onto the *ac* plane which are contained *within one repeat unit* in the *b* direction. The large and small discs indicate Ca and Na atoms, respectively, and their diameters are drawn in proportion to the square root of the scattering factors of Ca and Na atoms. Antiphase domain boundaries corresponding to Fig. 9 are indicated by dotted lines.

The optical diffractogram from this model does not correspond to the electron diffractogram shown in Fig. 10(*c*) but shows satellites with very different positions and intensities as shown in Fig. 10(*d*). Geometrical correspondence, however, is obtained for the optical diffractogram shown in Fig. 10(*e*). This pattern was obtained from the model shown in Fig. 10(*b*). The differences between the models shown in Figs. 10(*a*) and (*b*) are schematically drawn in Fig. 11. Ca and Na atoms on either side of antiphase boundaries replace each other as follows:

Ca atoms 3 are replaced by Na in subcells No. 1 and 2

Na atoms 2′ are replaced by Ca in subcells No. 1 and 2

Ca atoms 1 are replaced by Na in subcells No. 8 and 9

Na atoms 4′ are replaced by Ca in subcells No. 8 and 9

Na atoms 3 are replaced by Ca in subcells No. 10 and 11

Ca atoms 2′ are replaced by Na in subcells No. 10 and 11

Na atoms 1 are replaced by Ca in subcells No. 17 and 18

Ca atoms 4′ are replaced by Na in subcells No. 17 and 18.

If this procedure is applied to all antiphase boundaries, Fig. 10(*b*) is obtained. With this refined model and the consideration of nine layers in the *b* direction, Fig. 12(*a*) is obtained, and the optical diffractogram Fig. 12(*b*) shows an even better correspondence to the electron diffraction pattern. In this model the diameter of the discs is made proportional to the number of superpositions of Ca and Na atoms. The largest discs

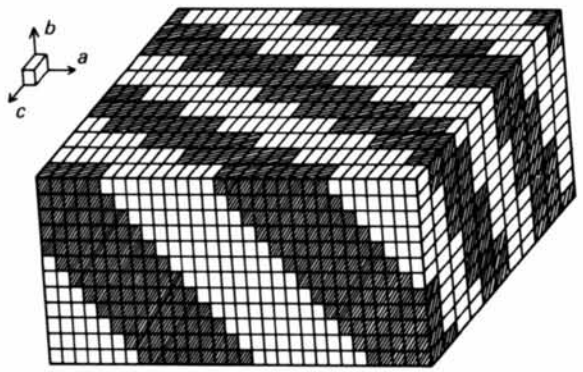

Fig. 9. Schematic representation of the model for An50 labradorite. Ca and Na atom arrangement in white and shaded regions are in antiphase relation.

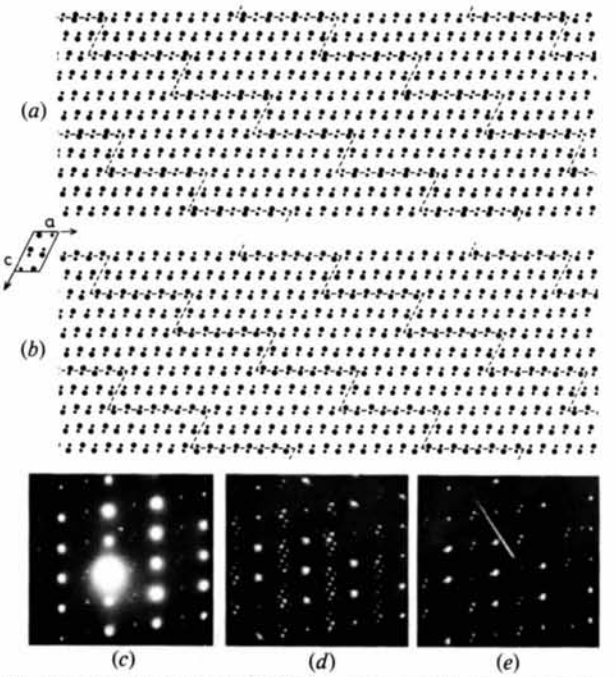

Fig. 10. The arrangements of Ca/Na atoms within one layer in the [010] projection. (*a*) A model not considering the configuration anomaly of Ca/Na in the antiphase boundaries. The boundaries corresponding to Fig. 9 are drawn as dotted lines. (*b*) A refined model, where Ca and Na are positioned near the boundaries in accordance with the rule of replacement. (*c*) Electron diffraction pattern of labradorite oriented with its axis [010] parallel to the electron beam. (*d*), (*e*) Optical diffractograms of the models in (*a*) and (*b*), respectively.

denote the superposition of nine Ca atoms and the smallest ones of nine Na atoms. The diameters for all other atom columns are equal to the average values of the scattering amplitude contributed from all Ca and Na atoms in the projected atom column. As can be seen from Fig. 12(*a*), the superposition of approximately equal amounts of Ca and Na atoms only occurs in the region midway between two antiphase domain boundaries.

The models for Ca and Na positions for the projections along [311], [131] and [5$\bar{1}$1], Figs. 5(*b*), 6(*b*) and 7(*b*), were drawn in accordance with the refined model. In these diffraction models, the proportion of the diameters is kept constant regardless of the thickness, because identical superposition of Ca and Na atoms occurs every three layers for the [311] and [131] projections and every five layers for the [5$\bar{1}$1] projection.

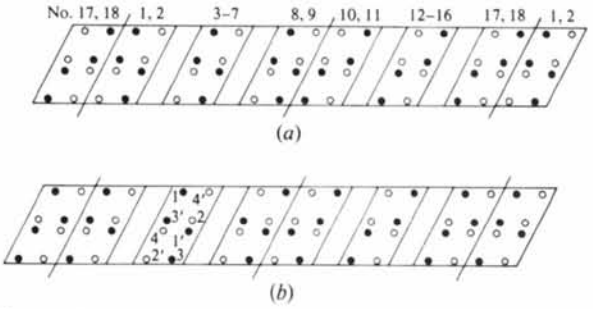

Fig. 11. Occupancies of Ca and Na atoms in one layer. Projection onto (010). Ca and Na atoms are represented as black and open circles, respectively. (*a*) Simple model shown in Fig. 10(*a*). (*b*) Refined model shown in Fig. 10(*b*).

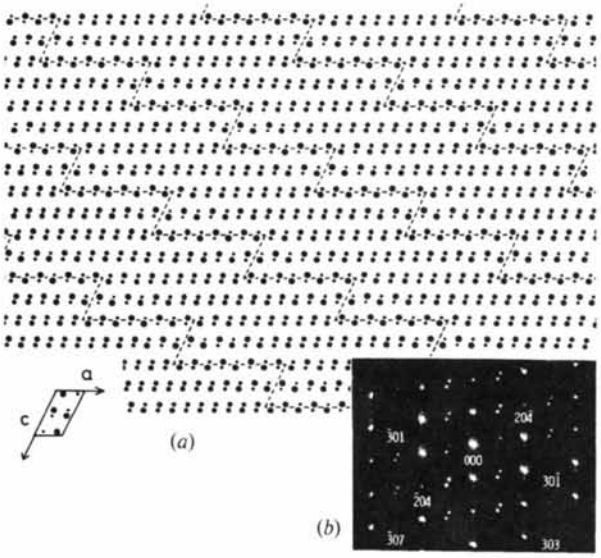

Fig. 12. (*a*) The arrangement of Ca/Na atoms within nine layers projected onto the plane normal to the axis [010]. The refined model is used. (*b*) Optical diffractogram of the model in (*a*).

With the model proposed in this section, good agreement in the positions of reflections is obtained between the optical and the electron diffraction patterns for all four projections. Some intensities are, however, missing or very weak in the optical diffraction patterns of the model. In Fig. 12(*b*), the satellite pairs around 303 and 3$\bar{0}$7 are missing. These extinctions are attributed to periodic weakening of intensity associated with the effect of disc size as mentioned in § 3. On the other hand, the reflections 20$\bar{4}$ and $\bar{2}$04 are very weak relative to the other *a* reflections, and 30$\bar{1}$ and $\bar{3}$01 are missing. The extinctions or quasi-extinctions of these reflections can be explained by considering the diffraction due to a pair of holes. We take the case that a number of pairs of circular holes with distance d is placed at regular intervals of D on a straight line. Although the diffraction pattern is a set of straight lines perpendicular to the row of holes and equally spaced at intervals of $1/D$, the intensities at $1/2d$, $3/2d$, $5/2d$, ... do not appear. The typical example is seen in Fig. 7(*e*), *i.e.* the diffraction spots higher than 033 disappear. The weakening or absence of reflections due to this effect is similarly seen in Figs. 5(*e*), 6(*e*), 10(*d*) and 10(*e*).

7. The role of the Al/Si tetrahedra

As the next step in the analysis, the atomic positions of Al and Si were included in the model. Al and Si were assumed to have the same scattering amplitude. The resulting pattern showing all atoms contained within nine layers in the [010] direction is presented in Fig. 13(*a*), and the corresponding optical diffraction pattern is given in Fig. 13(*b*). Except for the reflections 20$\bar{4}$ and $\bar{2}$04, Fig. 13(*b*) is almost identical to Fig. 12(*b*). It can therefore be concluded that the Al and Si atoms (even considering the small scattering difference between Al and Si) do not decisively influence the positions of reflection spots. The only exception is the pair of reflections 20$\bar{4}$ and $\bar{2}$04. These intensities are missing in Fig. 10(*e*) (simplified model with only Ca/Na) and are very weak in Fig. 12(*a*) (imposed model with only Ca/Na), but they are the strongest intensities in Fig. 13(*b*), where Al or Si, as well as Ca/Na, positions are included in the model. In this model, the two discs nearest to each other representing Ca/Na atoms do not appear any longer as a pair of holes. Therefore, the extinction of the optical diffraction intensities caused by a pair of holes is eliminated. Thus, when Al/Si positions are included, full agreement between optical diffraction and electron diffraction is obtained. The influence of the tetrahedral atoms on the optical diffraction pattern can therefore not be neglected. However, the ordering pattern of Al/Si should have a much smaller influence on the optical diffraction intensities than the Ca/Na

ordering pattern as a result of the small differences in scattering amplitude between Al and Si.

Since the electron scattering amplitude of oxygen atoms is $\frac{1}{3}$ of that for Al and Si atoms and oxygen atoms appear to have no positional changes in the antiphase boundary, the influence of the oxygen atoms was not tested in the present study. It is, however, possible that the modulation involving Ca/Na as well as Al/Si occupancy causes a weak modulation not only of the centers of tetrahedra but also of the rotational positions of the tetrahedra and thus an influence on the electron diffraction intensities could exist.

8. Discussion

Various models of labradorite based on X-ray diffraction have been proposed by Toman & Frueh (1976*a*,*b*), Kitamura & Morimoto (1977) and Korekawa & his collaborators (Korekawa & Jagodzinski, 1967; Korekawa & Horst, 1974; Korekawa, Horst & Tagai, 1978), but the models are rather different. In this paper, a new model of An50, especially for the positions of Ca and Na atoms, derived from high-resolution electron micrographs, electron diffraction patterns and optical diffractograms is presented.

Since it is difficult, at the present moment, to make a complete contrast calculation of the electron micrographs, the tentative contrast interpretation was made by an approximation to the many-beam dynamical theory of electron diffraction which suggests that Ca atoms appear darker than Na atoms, and Al and Si atoms appear with the same intensity. From these results, it was concluded that the alternating regions of darker and lighter contrast observed along the rows of dark spots in Figs. 5(*a*), 6(*a*) and 7(*a*) represent differences in the projected electric potential and are due to a preference for Ca and Na respectively in the occupancy of nontetrahedral cations.

On the other hand, optical diffraction patterns were useful in suggesting the occupancy of Ca/Na atoms in the antiphase boundary (114) when it is not parallel to the incident beam. In our model a special direction with regard to the Ca/Na occupancy exists. It deviates slightly from the *a* axis and has the index $[14,0,\bar{1}]$. Viewed along this axis, as shown in Fig. 14, the columns of nontetrahedral atoms will contain either Ca atoms only or Na atoms only.

In the present observation, specimens of An54 were used and for the determination of atom positions, the data of An55 (Toman & Frueh, 1973*a*) were used. The optical models were prepared by assuming An50 with no structural point defects. In the electron microscopic images shown in Figs. 5, 6, 7 and 13, many point-contrast anomalies randomly distributed can be seen, which appear to be due to compositional point defects. In general, although these defects can be seen in electron micrographs as contrast anomalies, they can hardly be detected in the diffraction patterns. Therefore, in the present observations, the difference of Ca and Na atom positions of An50 and An54 may not be well discerned if it can be assumed that the specimens contain the corresponding number of point defects in random distribution.

Complete image contrast calculations based on the many-beam dynamical theory of electron diffraction and image formation theory are now being carried out with the model proposed in the present paper and other published models. This paper stresses the importance of high-resolution electron micrographs, electron diffraction patterns and optical diffraction techniques as an aid in the analysis of complicated crystal structures including domains and superstructures, even though the limitations of the optical diffraction method should be recognized.

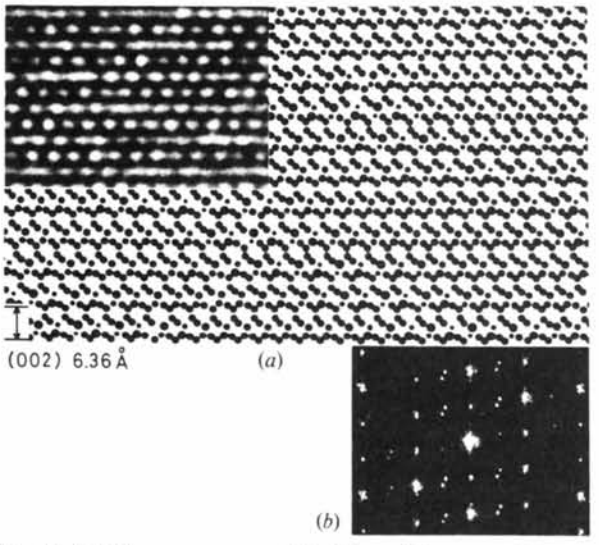

Fig. 13. (*a*) The arrangement of Ca, Na and T atoms within nine layers in the [010] projection, obtained by using the refined model. The electron micrograph is inserted at the same scale. (*b*) Optical diffraction pattern of the model in (*a*).

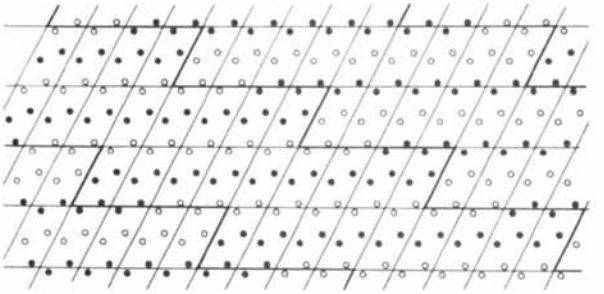

Fig. 14. The arrangement of Ca and Na atoms in the layer $-0{\cdot}03 < y < 0{\cdot}03$. Black and open circles indicate Ca and Na atoms, respectively. [010] projection.

The authors are indebted to Professor J. M. Cowley and Dr C. F. Woensdregt for helpful discussions, both orally and written, and to Mr A. Ono of the JEOL company for taking the electron micrographs in Figs. 6, 7 and 13, and Mr R. Wessicken of ETH Zürich for this collaboration.

References

BOWN, M. G. & GAY, P. (1958). *Z. Kristallogr.* **111**, 1–14.

COWLEY, J. M. (1959). *Acta Cryst.* **12**, 367–375.

GROVE, T. L. (1977). *Am. Mineral.* **62**, 932–941.

HASHIMOTO, H., KUMAO, A., ENDOH, H., NISSEN, H.-U., ONO, A. & WATANABE, E. (1975). *Proceedings of the EMAG Conference, Bristol*, pp. 245–250.

HASHIMOTO, H., NISSEN, H.-U., ONO, A., KUMAO, A., ENDOH, H. & WOENSDREGT, C. F. (1976). *Electron Microscopy in Mineralogy*, edited by H.-R. WENK *et al.* pp. 331–344. Berlin: Springer-Verlag.

JAGODZINSKI, H. & KOREKAWA, M. (1976). *Z. Kristallogr.* **143**, 239–277.

JAGODZINSKI, H. & KOREKAWA, M. (1978). *Phys. Chem. Miner.* **3**, 69–72.

KITAMURA, M. & MORIMOTO, N. (1977). *Phys. Chem. Miner.* **1**, 199–212.

KLEIN, S. & KOREKAWA, M. (1976). *Neues Jahrb. Mineral. Monatsh.* **H.2**, 66–69.

KOREKAWA, M. & HORST, W. (1974). *Fortschr. Mineral.* **52**, 37–40.

KOREKAWA, M., HORST, W. & TAGAI, T. (1978). *Phys. Chem. Miner.* **3**, 74–75.

KOREKAWA, M. & JAGODZINSKI, H. (1967). *Schweiz. Mineral. Petrogr. Mitt.* **47**, 269–278.

LIPSON, H. (1972). *Optical Transforms*. London, New York: Academic Press.

MCCONNELL, J. D. C. (1974). *The Feldspars*, edited by W. S. MACKENZIE & J. ZUSSMAN, pp. 478–490. Manchester Univ. Press.

MCLAREN, A. C. & MARSHALL, D. B. (1974). *Contrib. Mineral. Petrol.* **44**, 237–249.

MEGAW, H. D. (1960). *Proc. R. Soc. London Ser. A*, **259**, 59–78, 159–183, 184–202.

MORIMOTO, N., KITAMURA, M. & NAKAJIMA, Y. (1975). *Proc. Jpn Acad.* **51**, 729–732.

MORIMOTO, N., NAKAJIMA, Y. & KITAMURA, M. (1975). *Proc. Jpn Acad.* **51**, 725–728.

SCHERZER, O. (1949). *J. Appl. Phys.* **20**, 20–29.

TANJI, T. & HASHIMOTO, H. (1978). *Acta Cryst.* A**34**, 453–459.

TOMAN, K. & FRUEH, A. J. (1973*a*). *Z. Kristallogr.* **138**, 337–342.

TOMAN, K. & FRUEH, A. J. (1973*b*). *Acta Cryst.* A**29**, 127–133.

TOMAN, K. & FRUEH, A. J. (1976*a*). *Acta Cryst.* B**32**, 521–525.

TOMAN, K. & FRUEH, A. J. (1976*b*). *Acta Cryst.* B**32**, 526–538.

WENK, E., WENK, H.-R., GLAUSER, A. & SCHWANDER, H. (1975). *Contrib. Mineral. Petrol.* **53**, 311–326.

WENK, H.-R. (1978). *Proceedings of the 9th International Congress on Electron Microscopy, Toronto*, Vol. 3, pp. 404–419.

Acta Cryst. (1981). A**37**, 238–241

The Observation of Forbidden Reflections in V_3Si*

BY BERNARD BORIE

The Metals and Ceramics Division, Oak Ridge National Laboratory, Oak Ridge, Tennessee 37830, *USA*

(*Received* 16 *July* 1980; *accepted* 7 *October* 1980)

Abstract

Structurally forbidden Bragg maxima in the X-ray diffraction pattern of V_3Si have been observed. These reflections are excited by nonspherical electron distributions and anharmonic and anisotropic thermal motion. The forbidden reflections which are accessible to such excitation are correctly predicted by theory. Further studies of such maxima both with neutrons and X-rays should provide insights into the electronic and thermal behaviour of A15 compounds.

* Research sponsored by the Material Sciences Division, US Department of Energy under contract W-7405-eng-26 with the Union Carbide Corporation.

0567-7394/81/020238-04$01.00

Introduction

There has been recent interest in the experimental observation of structurally forbidden Bragg maxima from simple crystals. These very weak reflections have been found in the X-ray patterns of diamond (Bragg, 1921), silicon (Roberto & Batterman, 1970), germanium (Colella & Merlini, 1966), zinc (Merisalo, Järvinen & Kurittu, 1978) and both allotropes of tin (Field, 1976; Bilderback & Colella, 1975). Their measurement is useful because they are direct indications of anharmonic and anisotropic thermal motion and nonspherical electron distributions about nuclei. Though these phenomena are expected to cause